A Composite Gold−Silicon Oxide Surface for Mesoscopic Patterning

Keren Shabtai,[†] Sidney R. Cohen,[‡] Hagai Cohen,[‡] and Israel Rubinstein*[,†]

Department of Materials and Interfaces and Chemical Services Department, Weizmann Institute of Science, Rehovot 76100, Israel

Received: November 7, 2002; In Final Form: March 6, 2003

A composite surface comprising evenly distributed silicon oxide islands on a gold substrate is described. The composite surface is prepared by evaporation of a thin (50 nm) gold layer on oxide-free (H-passivated) silicon, followed by thermal diffusion of Si through the Au layer, gradually forming islands of SiO_2 on the Au surface. The rate of Si diffusion through the Au, and hence, the rate of SiO_2 island formation, is controlled by the annealing temperature, the Si crystallographic face, the Au film thickness, and the contacting atmosphere. The Au−SiO_2 composite surfaces can be used in applications requiring substrates patterned on a mesoscopic scale, while exposing two chemically dissimilar phases. One such application is shown here, namely, the formation of thiol−silane monolayers, for which the distribution of the different molecules in the resultant monolayer is determined by the substrate composition. The XPS controlled surface charging (CSC) method is used to establish a site-selective adsorption. The SiO_2 islands are found to be rather labile, shifting and aggregating upon self-assembly of alkanethiol molecules on the Au exposed areas. Pretreatment of the islands with a long-chain silane stabilizes the morphology.

Introduction

Controlled patterning of surfaces to obtain desired mesoscopic arrangements of materials of dissimilar properties presents a major thrust in basic and applied science where the goal is to provide novel arrays of electronic, optical, sensing, or biological elements, as well as platforms for new catalysts. Some of the approaches presented in recent years for bottom-up fabrication of mesoscopically patterned surfaces are given in refs 1−5 and references therein.

In most cases patterning is the first step in a more complex scheme that includes binding of different chemical or biological species to the different sites in the array, or patterned binding of a single species. The specific distribution of the bound species, determined by the array geometry, is then used for the desired purpose. Hence, the properties required of a mesoscopically patterned surface usually include (i) convenient preparation, (ii) control of the pattern geometry (possibly on different size scales), (iii) binding capability, and (iv) selective chemical reactivity of the different surface components.

Here we present a mesoscopically patterned surface that fulfils the above requirements. The system is composed of silicon oxide islands distributed on a gold surface. The composite surface is convenient to prepare, the surface composition can be controlled, and the two components (Au and SiO_2) display a substantially different chemical reactivity. Our preparative approach is based on diffusion of silicon through a layer of Au evaporated on a Si substrate. The Si diffuses from the Si/Au interface across the Au layer to reach the Au/air interface, where it is oxidized by ambient oxygen to form SiO_2 islands on the Au surface, which gradually cover the entire surface.

The Si/Au interface properties are determined by the procedure used for cleaning the Si substrates prior to Au deposition. The growth of a silicide from the Au film on the Si substrate requires that diffusion across the interface is not disturbed. The presence of a Si oxide layer at the interface is known to hinder the diffusion across the interface. Good adhesion of the Au to the Si substrate is obtained when the Au is evaporated *on a bare Si surface*, promoting silicide formation and Si out-diffusion. In contrast, the presence of a thin native Si oxide (always existing on Si in air) between the Au and the Si decreases substantially the adhesion of the Au layer,[6] preventing silicide formation and Si out-diffusion (Figure 1, parts a and b).

Oxide-free, H-passivated Si surfaces can be obtained by etching Si/Si-oxide substrates in HF,[7−10] HF mixed with nitric and acetic acids,[11,12] or HF mixed with NH_4F.[13] The procedure used here, i.e., treating the Si substrates with HF and carefully removing the dry, hydrophobic Si substrates from the solution without water rinse, produces H-terminated, oxide-free Si surfaces stable for up to ca. 30 min under ambient conditions.

The Si/Au interface has been extensively investigated. One of the most important properties is its diffusive character.[6,14,15] When bare Si is in contact with some metals (in our case, evaporated Au), it readily reacts with the metal at low temperatures (∼100 °C or below). Si atoms at the Si/Au interface are dislodged from the tightly bound Si crystal and diffuse through the Au film to the surface (possibly at grain boundaries) where they are oxidized. The rate of diffusion of Si through Au to form SiO_2 on the surface depends on the temperature, the contacting atmosphere (oxygen, humidity), and the Si crystallographic face.[11,12,15−22]

Several models for the low-temperature breaking of Si bonds, assisted by metal deposition, have been proposed.[23−28] The out-diffusion of Si from the Si/Au interface involves (i) bonding of interface Si atoms to Au and (ii) breaking of Si−Si bonds in the Si lattice. At the Si(100)/Au interface, two Si−Au bonds are formed and two Si−Si bonds must be broken to release Si. Hence, it is energetically more favorable for Si out-diffusion

* To whom correspondence should be addressed. Fax: +972-8-9344137. E-mail: israel.rubinstein@weizmann.ac.il.
[†] Department of Materials and Interfaces, Weizmann Institute of Science.
[‡] Chemical Services Department, Weizmann Institute of Science.

10.1021/jp022378k CCC: $25.00
Published on Web 05/20/2003

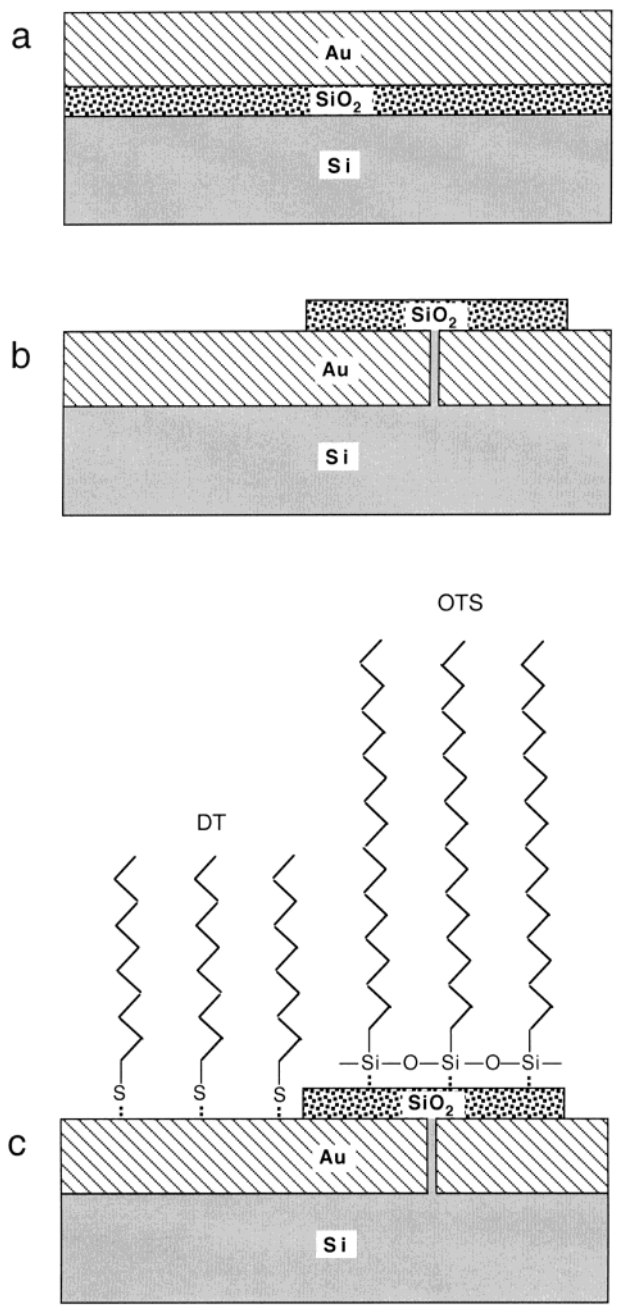

Figure 1. Schematic representation of the studied systems. (a) Au evaporated on Si/SiO_2 and annealed. (b) Au evaporated on oxide-free (H-passivated) Si and annealed. (c) A mixed silane−thiol monolayer self-assembled on a composite $Au-SiO_2$ surface.

than the Si(111)/Au interface, where only one Si−Au bond is formed and three Si−Si bonds must be broken.[22]

Here composite $Au-SiO_2$ surfaces are prepared by evaporation of 50 nm Au on oxide-free Si substrates. Upon moderate annealing the Si diffuses through the Au layer, gradually covering the Au surface. By changing the annealing time/temperature and the postannealing exposure to air, different surface compositions can be prepared. As a demonstration of possible applications, the composite surfaces are used here to obtain a controlled monolayer distribution.

Monolayer patterning is an important issue in itself,[29−31] mainly for reasons related to nanomaterial multitasking and the construction of future nanocomponent arrays. The $Au-SiO_2$ composite surface is well suited for monolayer patterning, using the two most common types of self-assembled monolayer headgroups, i.e., sulfur-based (thiols, disulfides, etc.), which bind preferentially to Au, and silanes, which bind preferentially to oxide surfaces. When the $Au-SiO_2$ surface is exposed to, e.g., a thiol molecule and a silane molecule (either simultaneously or consecutively), the distribution of the two components in the resultant monolayer is determined by the surface composition (Figure 1, part c), as we have recently demonstrated.[32]

In the present work, the preparation of $Au-SiO_2$ composite surfaces and the dependence of the surface structure on various parameters (annealing temperature and time, exposure to air, and the Si crystallographic face) are described in detail. The resulting surfaces are characterized using atomic force microscope (AFM) imaging, X-ray photoelectron spectroscopy (XPS), Cu underpotential deposition (UPD), and AC-impedance spectroscopy (ACIS). The use of the composite surfaces for monolayer patterning is discussed.

Experimental Section

Chemicals. Decanethiol (DT) (Aldrich) was passed twice through a column of silica gel with hexane as the solvent, followed by evaporation of the hexane. Chloroform (Biolab, AR) and bicyclohexyl (BCH) (Aldrich, AR) were passed through a column of activated basic alumina (Alumina B, Akt. 1, ICN). *n*-Octadecyltrichlorosilane (OTS) (Merck), HF (Merck, 40%), ethanol (Merck or Biolab, AR), H_2O_2 (Merck), NaOH (Merck, AR), H_2SO_4 (Palacid, 95−98%), Na_2SO_4 (Merck, AR), $CuSO_4$ (Merck, AR), $Fe_2(SO_4)_3$ (Fluka, AR), $FeSO_4$ (BDH, AnalaR), and liquid nitrogen were used as received. Water was triply distilled. Gases used were argon (99.996%), nitrogen (99.999%), and dry purified air.

Composite Surface Preparation. Optically polished p-type single crystal (111) silicon wafers (20−30 ohm.cm, Aurel GMBH, Landsberg, Germany) and n-type single crystal (100) silicon wafers (0.02−0.1 Ω cm, International Wafer Service) were cut into $\sim 2.2 \times 1.0$ cm^2 slides. The slides were sonicated 10 min in absolute ethanol and washed with triply distilled water. They were then left in a 0.5 M NaOH/10% H_2O_2 solution for 10 min, washed as above and left in a 33% H_2SO_4/10% H_2O_2 solution for 10 min, and washed as above and left in water at 90 °C for 30 min. The slides were then etched in 10% HF solution for 13 s, removed from the solution, blown dry under an argon stream, and immediately loaded into the evaporator chamber. The maximum time between etching and loading was 6 min.

Gold films, 50 nm thick, were deposited on the cleaned/etched Si substrates by mounting the slides in a cryo-HV evaporator (Key High Vaccum) equipped with a Maxtek TM-100 thickness monitor. Homogeneous deposition was obtained by moderate rotation of the substrate plate. Gold (99.99%) was evaporated from a tungsten boat at $(2-4) \times 10^{-6}$ Torr at a deposition rate of 0.1 nm/s. The temperature during deposition varied between 40 and 140 °C.

Postdeposition thermal treatment (annealing) of Au-covered Si slides was carried out in air (NEYTECH 85P furnace), at 150 °C for 12−48 min. The heating rate was 5 °C/min. The slides were left to cool to ambient temperature and stored in liquid nitrogen or under argon atmosphere.

Before use, some of the Au covered substrates were exposed to UV/ozone treatment for 10 min (UVOCS T10 × 10/OES/E), then immersed for 10 min in pure ethanol. The UV/ozone treatment cleans the surface and enhances the oxidation of the silica islands,[33−35] while the ethanol dip reduces the Au oxide formed during the UV/ozone exposure.[36]

Self-Assembled Monolayers (SAMs). Decanethiol (DT) SAMs were prepared by immersion of the substrates in a solution of 4 mM DT in BCH for 2 h (unless specified otherwise). The slides were rinsed with dry chloroform and dried under a stream of purified air.

n-Octadecyltrichlorosilane (OTS) SAMs were prepared by immersion of the substrates (pretreated by UV/ozone + ethanol dip, followed by exposure to water vapor[37]) in a solution of 2 mM OTS in BCH for 2 min. The slides were rinsed with dry chloroform and dried under a stream of purified air.

Mixed monolayers were prepared either by consecutive adsorption following the above procedures or by 2 min adsorption from a mixed OTS (2 mM) + DT (4 mM) solution in BCH followed by rinsing with dry chloroform and drying under a stream of purified air.

Atomic Force Microscope (AFM) Measurements. AFM images were obtained using a Topometrix TMX2010 Discoverer with a microfabricated integrated Si cantilever/tip (Nanosensors). The measurements were performed using semicontact mode in air at room temperature. The average diameter of the SiO_2 islands was estimated from the images as follows: For samples with short annealing (12 min) times, the median particle size was calculated using the public domain software package imageJ, a java-based version of the image package developed at NIH by Wayne Rasband, http://rsb.info.nih.gov. After importing the original Topometrix files into this package, the density-slice-defined particles were analyzed to find the area of each particle in the image while setting an upper limit on the particle size analyzed in order to avoid counting larger clusters. The resulting data set was imported into MS Excel, and the median value and standard deviation of the areas were calculated. The median particle diameter was then calculated by presuming a circular shape. To deduce the true particle radius R_P from that observed in the image, the probe tip radius was taken into account using the formula[38]

$$R_P = (w^2 + 4h^2)/8h - R_T$$

where w is the measured particle width in the image, h its height, and R_T the tip radius. This equation is valid for the present case, where R_T and R_P are similar in size. For samples annealed for longer times (24 min), the densely packed structure could not be reliably analyzed in this way, so approximate values were obtained by manually measuring a statistical sample of particles.

Scanning Electron Microscopy (SEM). SEM imaging was carried out with a JEOL JSM-6400F cold field emission scanning microscope.

X-ray Photoelectron Spectroscopy (XPS). XPS measurements were carried out with a Kratos Axis-HS system using monochromated Al Kα source at 75 W. Detection at a normal takeoff angle was applied with pass-energies ranging between 20 and 80 eV. Ar ion sputtering was performed with a 4 keV beam at a sputter rate of 50 A/min as determined with a Ta_2O_5/Ta reference. Details on the controlled surface charging (CSC) method using the electron flood gun are given elsewhere.[32]

Cu Underpotential Deposition (UPD). Cu UPD was carried out by cyclic voltammetry of the gold-coated substrates in aqueous 1 mM $CuSO_4$ + 0.1 M Na_2SO_4 solution in the range +0.400 to −0.400 V vs mercurous sulfate reference electrode (MSE). A conventional three-electrode cell was used, with an MSE reference electrode and a platinum disk counter electrode. The potentiostat and electrochemical programmer were built at the Department of Chemistry, Technion, Haifa. The charge was determined by integration of the UPD stripping (anodic) peak.

TABLE 1: XPS Results: Raw Atomic Concentration (%) of Unannealed Samples, Comprising 50 nm Au Evaporated on Oxide-Free Si Substrates

no.	substrate	Si	Au	C	O
1	Au on Si (100)	2.1	67.7	23.4	6.2
2	Au on Si (111)	0.7	62.0	33.2	4.1
3	**1**, 1 week in air	18.6	16.1	17.2	48.1
4	**2**, 1 week in air	1.2	58.4	35.2	5.1

AC-Impedance Spectroscopy (ACIS). The redox system for the ACIS measurements was 5 mN $FeSO_4/Fe_2(SO_4)_3$ in 0.1 M H_2SO_4. A conventional three-electrode cell was used with a platinum disk as a counter/reference electrode. The experimental setup included a Solartron model 1250 frequency response analyzer and model 1286 potentiostat. The impedance was measured at seven discrete frequencies per decade in the range 0.01 Hz−65 kHz at an amplitude of 5 mV (rms) around the reversible potential.

Results and Discussion

Composite Gold−Silicon Oxide Surfaces. The tendency of Si to diffuse through Au is demonstrated in Table 1, where XPS results are shown for Si diffusion through a 50 nm Au film on oxide-free Si surfaces, without any thermal treatment. It is evident that, in the case of Si(100), the Si diffuses through the Au film even at room temperature, reaching the Au/air interface where it reacts spontaneously with oxygen to form silica islands. With Si(111) this process is very slow (see Introduction). Note that the initial values in Table 1 reflect diffusion occurring already during the gold evaporation, which naturally involves some local heating. In the following we restrict the discussion to the Au−Si(111) surface as it provides a better compositional stability.

The diffusion process is evidently temperature sensitive. As seen in Table 2, rows 1−3, annealing at 150 °C induces a substantial increase in the rate at which Si atoms reach the Au/air interface. The silica coverage evaluated by XPS gradually increases with annealing time, as seen in the coverage values in Table 2 (for details see ref 32, supplement). The Si/O atomic ratio is close to 0.5 in all cases, meaning that at least the outer part (down to the escape depth of the photoelectrons, ca. 2−3 nm) of the silica islands is composed of SiO_2. Correspondingly, the binding energy of the Si (2p) line is 103.3 eV (energy scale calibrated via the C (1s) at 284.8 eV). Table 2, row 4, shows that treatment of the composite surface with UV/ozone followed by ethanol dip, a pretreatment required for monolayer self-assembly on the surface,[36] does not induce any dramatic changes in the surface composition other than a slight additional oxidation of the silicon (compare rows 2 and 4 in Table 2).

The substrates used in all the experiments described below were 50 nm Au films evaporated on oxide-free Si(111) surfaces and annealed in air at 150 °C. These conditions were chosen in order to achieve relatively fast substrate preparation with reasonable control over the composition of the Au−SiO_2 surface.

Parts a and f of Figure 2 show AFM images of Au−SiO_2 composite surfaces, prepared as described above using 12 and 24 min annealing times, respectively, followed by UV/ozone + ethanol dip treatment. The SiO_2 islands are seen as bright spots distributed on the Au surface. The average island diameter in Figure 2a (12 min annealing), obtained as detailed in the Experimental Section, is 30 nm (the sizable spread in particle sizes gives a standard deviation of 25 nm). The average aspect ratio of the islands (height/diameter) is 0.5. For longer annealing periods (24 min, Figure 2, part f), both the number and size of the SiO_2 grains on the Au increase. The overall surface coverage

TABLE 2: XPS Results: Atomic Concentration (%) for Substrates Comprising 50 nm Au Evaporated on Oxide-Free Si(111) and Annealed at 150 °C[a]

no.	annealing time (min)	postannealing treatment	Si	Au	S	C	O	Si/O	C^{Au}/C^{Si}	SiO_2 coverage %
1	**12**		9.7	47.5		21.8	21.1	0.5	>5	32
2	**24**		16.4	38.0		16.7	28.9	0.6	1	52
3	**48**		22.1	21.0		11.2	45.7	0.5	0.3	75
4	**24**	10 min UV/ozone 10 min EtOH	13.1	40.5		15.9	30.4	0.43	1	52
5	**24**	10 min UV/ozone 10 min EtOH 2 h DT	9.5	31.2	1.5	31.0	26.9	0.4	1.85	48
6	**24**	10 min UV/ozone 10 min EtOH 2 min OTS	12.0	31.2		34.0	22.8	0.5	1	52
7	**24**	10 min UV/ozone 10 min EtOH 2 min OTS 2 h DT	13.7	26.5	1.8	37.3	20.7	0.7	0.92	52
8	**24**	10 min UV/ozone 10 min EtOH 2 h DT 2 min OTS	8.5	29.3	1.5	44.4	16.3	0.5	0.8	48

[a] Samples no. 4−8 were subsequently subjected to the indicated post-annealing processes. C^{Au}/C^{Si} relates the carbon line decomposition to signals associated with gold sites vs silica sites as derived by CSC.[32] The coverage values include corrections due to the attenuation introduced by the adsorbed carbon.

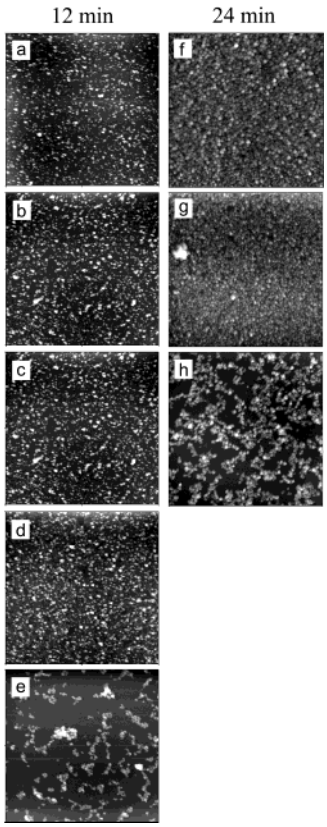

Figure 2. AFM images (5.0 μm × 5.0 μm, semicontact mode) of Si(111)/Au substrates, annealed in air 12 min (left) or 24 min (right) at 150 °C, then treated by UV/ozone and ethanol dip (a and f) followed by self-assembly of (b) OTS, (c) OTS followed by DT, (d) OTS + DT, (e) DT, (g) OTS followed by DT, and (h) DT followed by OTS. The *Z*-range (in nanometers) for parts a−h, respectively, is 49, 45, 45, 54, 74, 56, 84, and 61.

increases by a factor of 2−3, and the average particle size increases slightly to ca. 40 nm. A complementing picture of the 24 min annealed surface is seen in the SEM image in Figure 3 (top). The apparent lower density of islands in the SEM micrograph relative to the AFM image is due to selective charging (i.e., enhancement) of some of the SiO_2 particles.

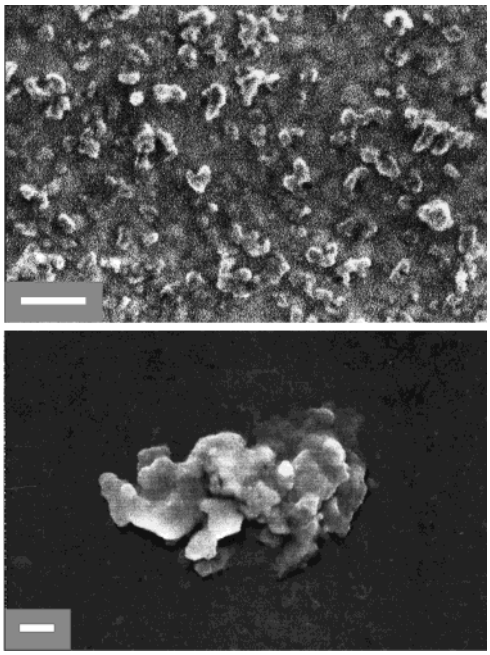

Figure 3. Top: SEM image of a Si(111)/Au substrate, annealed 24 min at 150 °C in air, then treated by UV/ozone and ethanol dip. Bottom: A similarly prepared substrate after self-assembly of DT for 7 min. Bars = 100 nm.

Figure 4 presents XPS depth-profiling results of a composite surface (annealed 48 min at 150 °C, see Table 2, row 3). The O/Si atomic ratio before sputtering is 2, which is an indication of the composition at the grain surface (SiO_2). Upon sputtering, this ratio gradually decreases, while the Si line broadens significantly to lower binding energies. Curve fitting of the Si (2s) line verifies that, in addition to SiO_2, the sputtering unveils unoxidized Si, associated with either grain cores or, more likely, with silicon dissolved within the gold.

Control of the SiO_2 Coverage. Quantitative assessment of the SiO_2 coverage was also carried out electrochemically, using two different approaches: (i) Cu underpotential deposition (UPD) and (ii) AC-impedance spectroscopy (ACIS). Determination of the SiO_2 coverage is based on the assumption that the

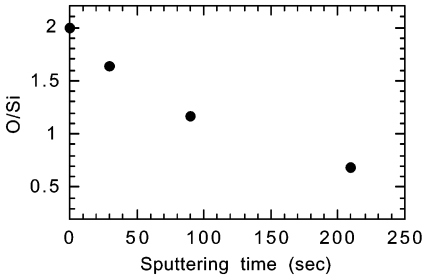

Figure 4. XPS depth profiling: O/Si atomic concentration ratio vs sputtering time for a Si(111)/Au substrate, annealed in air 48 min at 150 °C, then treated by UV/ozone and ethanol dip.

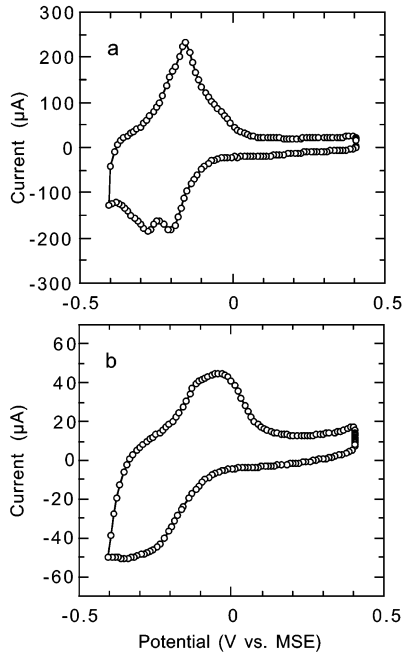

Figure 5. Cu UPD voltammograms (scan rate: 100 mV/s) in 1.0 mM $CuSO_4$ + 0.1 M Na_2SO_4 solution for (a) bare Au electrode (area: 1.1 cm^2) and (b) Si(111)/Au, annealed in air 48 min at 150 °C (area: 0.65 cm^2).

fraction of bare Au can serve as an electrode in redox reactions, while the fraction of the surface covered with insulating SiO_2 is inert. Similar quantitative analyses of surfaces partially covered with insulating layers using Cu UPD[39] and ACIS[40,41] were previously demonstrated; details on the methods and calculations can be found in the cited references.

The SiO_2 coverage can be controlled by the annealing time, as shown in Table 2, rows 1−3, and Figure 2, parts a and f. Another way of controlling the coverage is to leave the annealed sample at room temperature under ambient conditions for different periods of time. The SiO_2 coverage increases with time after annealing, and the surface composition can be frozen at any desired time by either applying sample cooling to liquid nitrogen temperature or by transferring the sample to an Ar atmosphere.

Figure 5 shows an example of Cu UPD curves used to determine the SiO_2 coverage. The fraction of gold surface covered by the insulating silica was determined by comparing the amount of charge required for Cu UPD at a composite electrode with that for a bare Au electrode.

Cu UPD results for postannealing changes in SiO_2 coverage are shown in Figure 6 where the fractional coverage increases systematically from ca. 30% to ca. 80%. These results do not contradict the data in Table 1, where unannealed Si(111) shows

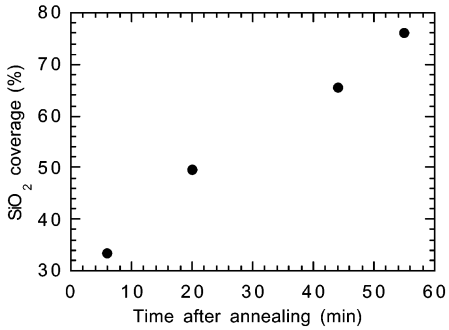

Figure 6. Cu UPD results: Fractional coverage (%) of SiO_2 on Si(111)/Au substrates vs time of exposure to air at room temperature following annealing in air, 48 min at 150 °C.

only negligible coverage changes even on a long-time scale. The annealing stage, initiating Si diffusion, necessarily leaves a profile of (nonoxidized) Si within the gold. Hence, the postannealing diffusion is associated with the Si portion situated relatively close to the surface, its diffusion motivated by the presence of external oxygen. Independent evidence for the existence of dissolved silicon in the gold is found in the XPS depth profile, where nonoxidized Si is observed, its signal increasing into the gold layer (Figure 4). Hence, the postannealing effect points to the role of the oxygen in driving the diffusion through the gold.

The change in the SiO_2 fractional coverage as a function of time after annealing was measured independently using ACIS.[40,41] Results of such an experiment are presented in Figure 7 as complex impedance plots. The systematic increase in the diameter of the semicircle with increasing time after annealing is interpreted as an increase in the charge-transfer resistance of the electrode reaction resulting from gradual coverage of the surface with an insulating phase. The fractional surface coverage is obtained by comparing the diameter of semicircle in the complex impedance plot of the composite electrode with that of the bare Au electrode (i.e., before annealing).[40,41]

Results of the ACIS experiments are shown in Figure 8 and compared with the respective Cu UPD results (data from Figure 6). The coverage results obtained by the two methods are in reasonable agreement, considering the relatively large margin for error in the sample preparation procedure. The results show that the surface composition can be controllably varied in the entire range of coverages.

It is quite intriguing that the electrochemical coverage values obtained immediately after annealing (Figures 6 and 8) are consistently lower than the values obtained by analysis of the XPS data (Table 2) as well as from qualitative assessment of the AFM images (Figure 2). A probable explanation is that the SiO_2 aggregates are partially porous, exposing a larger fraction of the Au to the solution compared to the coverage values derived by XPS or AFM, for which a two-dimensional projection of the whole structure determines the result.

Monolayer Self-Assembly. Au−SiO_2 composite surfaces were used as substrates for the preparation of mixed SAMs, such that the distribution of the two monolayer components is dictated by the surface composition. The mixed monolayers were prepared from decanethiol (DT) and octadecyltrichlorosilane (OTS) molecules. The former are expected to bind to the bare Au fraction while the latter are expected to bind to the SiO_2 islands as shown schematically in Figure 1, part c.[32]

Parts b−e, g, and h of Figure 2 show AFM images of composite surfaces following self-assembly of single-component (parts b and e) and two-component (parts c, d, g, and h)

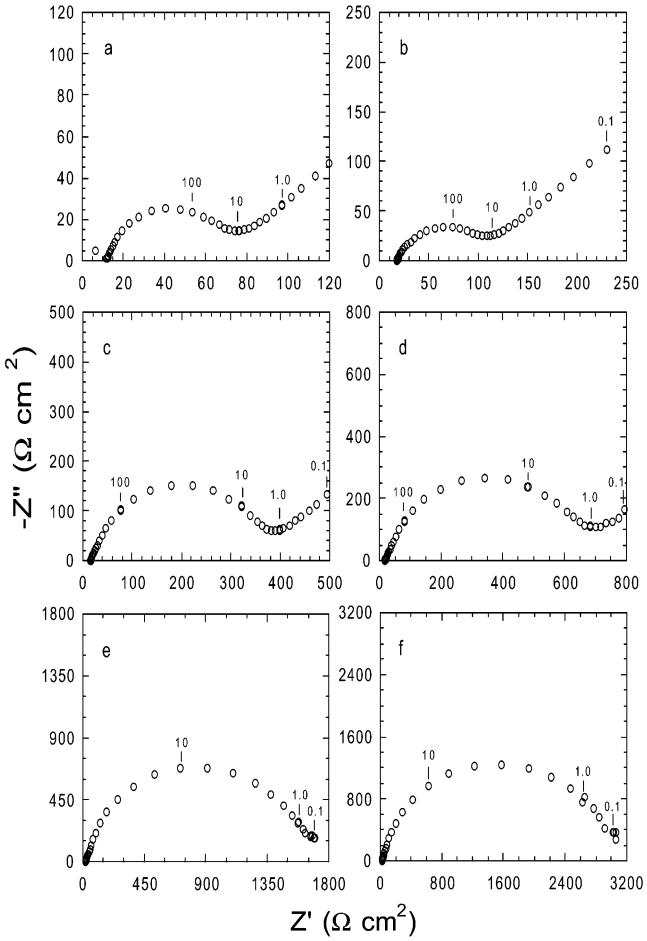

Figure 7. AC-impedance spectroscopy results: Complex impedance plots recorded in 0.5 mN $FeSO_4/Fe_2(SO_4)_3$ + 0.1 M H_2SO_4 for Si(111)/Au substrates before (a) annealing and after annealing 48 min at 150 °C, then leaving the samples in air at room temperature for (b) 18 min, (c) 48 min, (d) 60 min, (e) 93 min, and (f) 188 min. Frequency range: 0.1−65000 Hz; some frequencies are indicated as a guide.

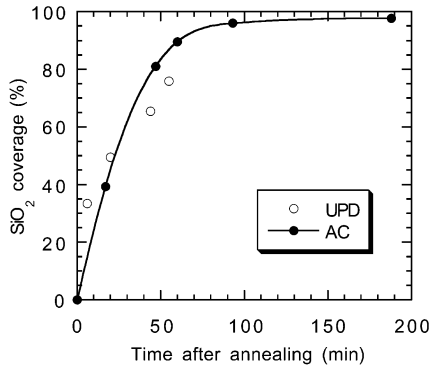

Figure 8. AC-impedance and Cu UPD results: Change in SiO_2 fractional coverage (%) vs time for Si(111)/Au substrates, annealed 48 min at 150 °C, then left in air at room temperature for different times. AC-impedance data extracted from Figure 7; Cu UPD data taken from Figure 6.

monolayers. In Figure 2, parts b, c, d, and g, the island distribution is similar to that of the bare composite surface (Figure 2, parts a and f), indicating that the OTS adsorption does not alter the surface morphology to a noticeable extent. On the other hand, exposure of the surface to DT alone (Figure 2, part e) or DT followed by OTS (Figure 2, part h) induces a substantial change in the SiO_2 island distribution, with extensive island dislocation, aggregation, and creation of new and different surface morphologies. A closeup of a typical aggregate of SiO_2

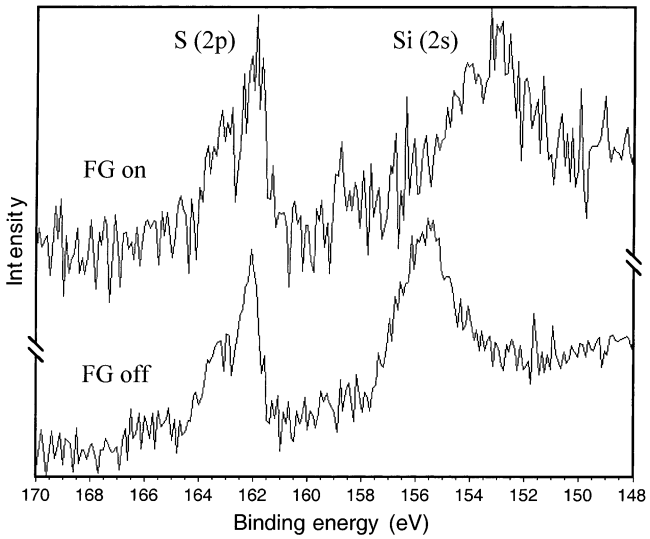

Figure 9. Controlled surface charging (CSC) in XPS, demonstrated with a Si(111)/Au substrate, annealed 12 min at 150 °C, followed by adsorption of a DT monolayer. The S (2p) and Si (2s) lines are shown; measurements with the electron flood gun in the "off" and "on" positions are indicated. Note the sizable shift of the Si (2s) signal. The slight shift of the S (2p) line, observed for the gold signal as well, is a result of finite wafer conductivity.

islands is shown in the SEM image in Figure 3 (bottom; compare with Figure 3, top), in which it is evident that even a relatively short (7 min) exposure to DT causes island dislocation and aggregation. This indicates that the adhesion of the islands to the Au is weak compared to that of the thiol. Therefore, islands can be shifted on the surface (and even partially removed) by the adsorbed thiol molecules to form new arrangements. The process is driven by repulsion between the hydrophobic (monolayer coated) Au surface and the hydrophilic SiO_2 islands, inducing larger continuous DT areas and SiO_2 aggregation. Note that binding of OTS to the SiO_2 (hence, creating hydrophobic grain surfaces) immobilizes the islands and suppresses their self-aggregation, such that the morphology is stabilized (see Figure 2, parts c, d, and g).

Table 2, rows 5−8, presents XPS results for the formation of single-component (rows 5 and 6) and two-component (rows 7 and 8) monolayers on composite surfaces. The results do not show any unusual or unexpected feature. The binding of the DT to the surface is indicated by the appearance of a sulfur peak in the spectra (rows 5, 7, and 8). The Si peak cannot be used to follow the binding of OTS, as it is a component of both OTS and the SiO_2 islands. However, the substantial increase in the carbon peak and the C/Au ratio in all cases (rows 5−8) is attributed to coverage of the surface with SAMs bearing alkyl chains. Note that the total amount of carbon in rows 6 and 7, Table 2, is quite similar, indicating the general tendency of gold surfaces to adsorb organic impurities; the latter are efficiently replaced by DT.

The distribution of the two monolayer components (thiol and silane) between the two types of surface sites (bare Au and SiO_2 islands) can be elucidated using the XPS controlled surface charging (CSC) method.[32,42] The method is based on the induction of electric fields onto the studied surface, which is accomplished by using the electron flood gun. By monitoring respective shifts in the binding energy of different elements in the XPS spectrum, an effective differentiation is achieved between signals originating from the different surface sites. In the present case, no shift indicates signals associated with conducting sites (i.e., open gold areas), while a pronounced shift

characterizes signals associated with insulating sites (i.e., the silica grains).[32]

Figure 9, in which the spectra for S and Si are shown, presents an example of such an experiment for a DT monolayer on a composite surface. No shift in the S peak indicates that the sulfur of the DT molecules is attached to the conducting (gold) sites. The shift in the Si peak to lower binding energies indicates that it originates from the insulating (SiO_2) regions, in which the local potential is easily varied by the applied charging. XPS results for this system are presented and discussed in more detail in ref 32.

Conclusions

The facile diffusion of Si in Au at moderate temperatures was exploited for the formation of composite surfaces comprising SiO_2 islands on an Au surface. The fraction of the surface occupied by SiO_2 islands can be systematically varied by selecting the Si crystallographic face, annealing temperature, time (annealing and/or postannealing), Au film thickness, and the contacting atmosphere. The process was followed quantitatively using XPS, as well as electrochemical methods, i.e., Cu UPD and ACIS. The morphology and composition of the $Au-SiO_2$ surfaces were characterized by AFM and XPS. Patterned substrates with nanometric features displaying distinct conductivity and chemical selectivity have been obtained. In the present work they were used as substrates for self-assembly of single-component or mixed monolayers, providing a template for rational distribution of the different monolayer constituents. The latter was shown using XPS controlled surface charging (CSC). The intriguing effect of thiol molecules in inducing SiO_2 island dislocation and redistribution on the Au surface, as well as the effect of silane molecules in stabilizing the surface morphology, requires further investigation.

Acknowledgment. We thank Dr. D. Mahalu for assisting with the SEM imaging. I.R. acknowledges support of this work from the US-Israel Binational Science Foundation and the Minerva Foundation, Munich.

References and Notes

(1) Zheng, J.; Zhu, Z.; Chen, H.; Liu, Z. *Langmuir* **2000**, *16*, 4409.
(2) Pfohl, T.; Kim, J. H.; Yasa, M.; Miler, H. P.; Wong, G. C. L.; Bringezu, F.; Wen, Z.; Wilson, L.; Kim, M. W.; Li, Y.; Safinya, C. R. *Langmuir* **2001**, *17*, 5343.
(3) Shimomura, M.; Sawadaishi, T. *Curr. Opin. Colloid Interface Sci*. **2001**, *6*, 11.
(4) Jacobs, H. O.; Tao, A. R.; Schwartz, A.; Gracias, D. H.; Whitesides, G. M. *Science* **2002**, *296*, 323.
(5) Rosei, F.; Schunack, M.; Jiang, P.; Gourdon, A.; Lægsgaard, E.; Stensgaard, I.; Joachim, C.; Besenbacher, F. *Science* **2002**, *296*, 328.
(6) Dallaporta, H.; Cros, A. *Surf. Sci.* **1986**, *169*, L355.
(7) Cros, A.; Muret, P. *Mater. Sci. Rep.* **1992**, *8*, 271.
(8) Golan, Y.; Margulis, L.; Matlis, S.; Rubinstein, I. *J. Electrochem. Soc*. **1995**, *142*, 1629.
(9) Cerfolini, G. F.; Meda, L. *Appl. Surf. Sci.* **1995**, *89*, 351.
(10) Stockhausen, A.; Kampen, T. U.; Mönch, W. *Appl. Surf. Sci.* **1992**, *56−58*, 795.
(11) Green, A. K.; Bauer, E. *J. Appl. Phys.* **1976**, *47*, 1284.
(12) Green, A. K.; Bauer, E. *J. Appl. Phys.* **1981**, *52*, 5098.
(13) Ye, J. H.; Kaji, K.; Itaya, K. *J. Electrochem. Soc.* **1996**, *143*, 4012.
(14) Cros, A.; Dallaporta, H.; Oberlin, J. C. *Appl. Surf. Sci.* **1992**, *56−58*, 434.
(15) Hiraki, A.; Nicolet, M.-A.; Mayer, J. W. *Appl. Phys. Lett.* **1971**, *18*, 178.
(16) Hiraki, A. *Surf. Sci. Reports* **1984**, *3*, 357.
(17) Hiraki, A. *Surf. Sci*. **1986**, *168*, 74.
(18) Hiraki, A.; Lugujjo, E.; Nicolet, M.-A.; Mayer, J. W. *Phys. Status Solidi A* **1971**, *7*, 401.
(19) Hiraki, A.; Lugujjo, E.; Mayer, J. W. *J. Appl. Phys*. **1972**, *43*, 3643.
(20) Narusawa, T.; Kinoshita, K.; Gibson, W. M.; Hiraki, A. *J. Vac. Sci. Technol.* **1981**, *18*, 872.
(21) Okuno, K.; Itoh, T.; Iwami, M.; Hiraki, H. *Solid State Commun*. **1980**, *34*, 493.
(22) Chang, C.-A.; Ottavini, G. *Appl. Phys. Lett*. **1984**, *44*, 901.
(23) Walser, R. W.; Bené, R. W. *Appl. Phys. Lett.* **1976**, *28*, 624.
(24) Tu, K. N. *Appl. Phys. Lett*. **1975**, *27*, 221.
(25) Hiraki, A. *J. Electrochem. Soc*. **1980**, *127*, 2662.
(26) Inkson, J. C. *Surf. Sci*. **1971**, *28*, 69.
(27) Meinel, K.; Katzer, D. *Appl. Surf. Sci*. **1992**, *56−58*, 514.
(28) Iwami, M.; Terada, T.; Tochihara, H.; Kubota, M.; Murata, Y. *Surf. Sci*. **1988**, *194*, 115.
(29) Laibinis, P. E.; Hickman, J. J.; Wrighton, M. S.; Whitesides, G. M. *Science* **1989**, *245*, 845.
(30) Kim, E.; Kumar, A.; Whitesides, G. M. *J. Electrochem. Soc*. **1995**, *142*, 628.
(31) Coda, M. E.; Du, H.; Bhandarkar, S.; Johnson, D. W. *Supramol. Sci*. **1997**, *4*, 43.
(32) Shabtai, K.; Rubinstein, I.; Cohen, S. R.; Cohen, H. *J. Am. Chem. Soc.* **2000**, *122*, 4959.
(33) Bruner, H.; Vallant, T.; Mayer, U.; Hoffmann, H. *Langmuir* **1996**, *12*, 4614.
(34) Haran, A.; Waldeck, D. H.; Naaman, R.; Moons, E.; Cahen, D. *Science* **1994**, *263*, 948.
(35) Niwano, M.; Suemitsu, M.; Ishibashi, Y.; Takeda, Y.; Miyamoto, N. *J. Vac. Sci. Technol. A* **1992**, *10*, 3171.
(36) Ron, H.; Matlis, S.; Rubinstein, I. *Langmuir* **1998**, *14*, 1116.
(37) Ulman, A. *An introduction to Ultrathin Organic Films*; Academic Press: New York, 1991; pp 245−253.
(38) Ramirez-Aguilar, K. A.; Rowlen, K. L. *Langmuir* **1998**, *14*, 2562.
(39) Gafni, Y.; Weizman, H.; Libman, J.; Shanzer, A.; Rubinstein, I. *Chem. Eur. J.* **1996**, *2*, 759.
(40) Sabatani, E.; Rubinstein, I. *J. Phys. Chem.* **1987**, *91*, 6663.
(41) Sabatani, E.; Cohen-Boulakia, J.; Bruening, M.; Rubinstein, I. *Langmuir* **1993**, *9*, 2974.
(42) Doron-Mor, I.; Hatzor, A.; Vaskevich, A.; van der Boom-Moav, T.; Shanzer, A.; Rubinstein, I.; Cohen, H. *Nature* **2000**, *406*, 382.